LETTER

A prefrontal cortex–brainstem neuronal projection that controls response to behavioural challenge

Melissa R. Warden[1], Aslihan Selimbeyoglu[1,2], Julie J. Mirzabekov[1], Maisie Lo[3], Kimberly R. Thompson[1], Sung-Yon Kim[1,2], Avishek Adhikari[1], Kay M. Tye[1,4], Loren M. Frank[5,6] & Karl Deisseroth[1,2,7,8,9]

The prefrontal cortex (PFC) is thought to participate in high-level control of the generation of behaviours (including the decision to execute actions[1]); indeed, imaging and lesion studies in human beings have revealed that PFC dysfunction can lead to either impulsive states with increased tendency to initiate action[2], or to amotivational states characterized by symptoms such as reduced activity, hopelessness and depressed mood[3]. Considering the opposite valence of these two phenotypes as well as the broad complexity of other tasks attributed to PFC, we sought to elucidate the PFC circuitry that favours effortful behavioural responses to challenging situations. Here we develop and use a quantitative method for the continuous assessment and control of active response to a behavioural challenge, synchronized with single-unit electrophysiology and optogenetics in freely moving rats. In recording from the medial PFC (mPFC), we observed that many neurons were not simply movement-related in their spike-firing patterns but instead were selectively modulated from moment to moment, according to the animal's decision to act in a challenging situation. Surprisingly, we next found that direct activation of principal neurons in the mPFC had no detectable causal effect on this behaviour. We tested whether this behaviour could be causally mediated by only a subclass of mPFC cells defined by specific downstream wiring. Indeed, by leveraging optogenetic projection-targeting to control cells with specific efferent wiring patterns, we found that selective activation of those mPFC cells projecting to the brainstem dorsal raphe nucleus (DRN), a serotonergic nucleus implicated in major depressive disorder[4], induced a profound, rapid and reversible effect on selection of the active behavioural state. These results may be of importance in understanding the neural circuitry underlying normal and pathological patterns of action selection and motivation in behaviour.

To execute an action that expends energy and requires vigorous effort under challenging conditions represents a consequential decision for an organism, particularly as such an action may not always represent the most adaptive behaviour. When a vigorous action pattern is selected despite extremely difficult circumstances (rather than a more energy-conserving passive or depressive-type pattern), an assessment may have occurred that the anticipated outcomes of the vigorous action would justify the expenditure of energy. Conversely, when an organism selects inactive behavioural patterns during challenging situations, the decision may represent anticipation that effort would probably be fruitless. Such anticipation leading to inaction can become maladaptive in human beings, with clinical symptoms including psychomotor retardation and hopelessness (core defining features of major depression, a disease with lifetime prevalence of nearly 20% and extensive socioeconomic ramifications[5]).

We sought to probe these high-level processes governing behavioural state selection with targeted control of restricted sets of circuit elements in freely moving mammals. Increasing evidence suggests that the prefrontal cortex (PFC) could be involved in these behaviours; the PFC is responsible for coordinating thought and action, and has been shown to be critical for goal-oriented behaviour, planning and cognitive control[6,7]—all of which are impaired in pathological states such as depression[8–11]. Moreover, deep brain stimulation of the subcallosal cingulate region elicits antidepressant effects in treatment-resistant patients[12]. Electrical stimulation of the rodent mPFC induces an antidepressant-like reduction in immobility in the forced swim test (FST)[13], optogenetic stimulation of mixed excitatory and inhibitory neural populations in mPFC has an antidepressant-like effect in social defeat[14], and mPFC in rodents has a role in mediating resilience[15]. Finally, neuroimaging studies in human patients have been instrumental in focusing attention on brain regions including PFC that exhibit abnormal activity in depression and melancholic states[3,16,17].

Despite these pioneering efforts exploring the role of the PFC, it is unclear which specific neural pathways are involved in real-time selection of effortful behavioural responses to challenging situations. The FST is relevant to this issue, as a widely employed behavioural test of depression-related responses in rodents[18]. In the FST, rodents are placed in a tank of water from which it is not possible to escape, and animals exhibit periods (epochs) of floating, which are thought to reflect states of passive coping or behavioural despair[18], interspersed with epochs of active escape behaviour. Immobility in the FST is influenced by antidepressant drugs[19] and stress[20]. Transitions between active-escape and behavioural-despair states in the FST are clearly demarcated, in principle providing an unambiguous, instantaneous classification of a specific motivated behavioural state and an opportunity to investigate the neural dynamics underlying the decision to adopt an active behavioural response to challenge. However, to our knowledge, neural activity has never been recorded in behaving animals during the FST because of the technical obstacles of recording and controlling neural activity in a freely swimming animal. To address this challenge, we developed new methods for recording millisecond-precision neural and behavioural data alongside optogenetic control during the FST (Fig. 1).

We designed a magnetic induction method to detect individual swim kicks, in which the FST tank of water was surrounded by an induction coil and a small magnet was attached to the hind paw of the subject animal (Fig. 1a). During the FST, each kick induced a current in the coil (Fig. 1b); it was possible to cleanly isolate single kicks (Supplementary Fig. 1), and both kick frequency and automatically scored immobility corresponded well to manually scored immobility (Fig. 1c, d). In addition, we used this method to record mobile and immobile states during cage activity (Supplementary Fig. 2). To record well-isolated single units during swimming, tetrode microdrives or fixed wire arrays were waterproofed (Supplementary Methods). Under these conditions, we were reliably able to isolate single units during the FST (Fig. 1e); indeed,

[1]Department of Bioengineering, Stanford University, Stanford, California 94305, USA. [2]Neurosciences Program, Stanford University, Stanford, California 94305, USA. [3]Bio-X Program, Stanford University, Stanford, California 94305, USA. [4]Picower Institute for Learning & Memory, Department of Brain & Cognitive Sciences, Massachusetts Institute of Technology, Cambridge, Massachusetts 02139, USA. [5]Department of Physiology, University of California San Francisco, San Francisco, California 94143, USA. [6]W.M. Keck Center for Integrative Neuroscience, University of California San Francisco, San Francisco, California 94143, USA. [7]Department of Psychiatry & Behavioral Sciences, Stanford University, Stanford, California 94305, USA. [8]CNC Program, Stanford University, Stanford, California 94305, USA. [9]Howard Hughes Medical Institute, Stanford University, Stanford, California 94305, USA.
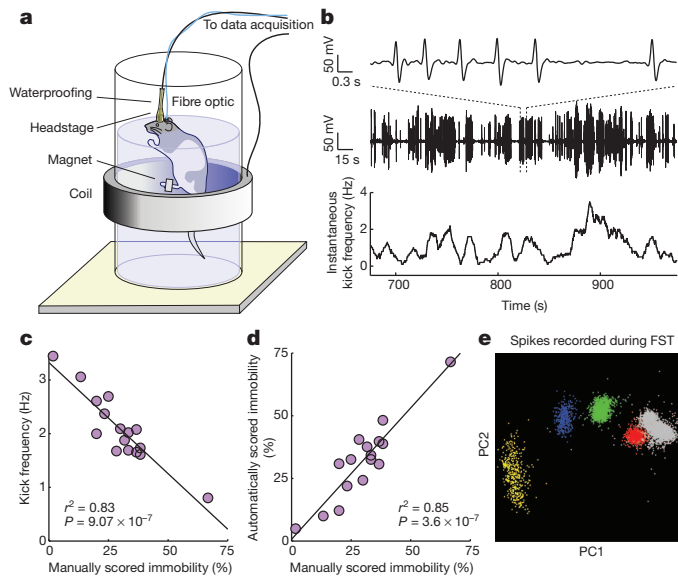
Figure 1 | The automated FST provides a high-temporal-resolution behavioural read-out that can be synchronized with simultaneously recorded neural data. a, A schematic of the automated FST. A coil of wire surrounds the tank of water and a magnet is attached to the rat's back paw. Movement of the magnet within the coil during swimming induces a current that can be recorded. To permit concurrent neural recordings, the headstage is waterproofed. An optical fibre can be included for simultaneous optical stimulation. **b**, Example FST coil voltage traces. Top, a 6-s coil trace showing individual kicks; middle, a 5-min coil trace; bottom, instantaneous kick frequency estimated from the 5-min coil trace. **c**, Average kick frequency corresponds well to manually scored immobility estimates. **d**, Estimates of FST immobility derived from the induction coil correspond tightly to manually scored immobility estimates. **e**, Four well-isolated single mPFC units recorded during the FST. PC, principal component (see Methods).

we were able to detect transitions between active escape behaviour and immobile states with high temporal precision, and to correlate these behaviours with ongoing neural activity (Fig. 2).

We recorded neural activity using either a 4-tetrode microdrive (6 rats) or a 24-electrode fixed-wire array (5 rats) targeted to the mPFC (Fig. 2a). Three epochs of data were recorded (Fig. 2b): a 15-min pre-FST epoch in a familiar cage, a 15-min epoch during the FST, and a 15-min post-FST epoch. We found that many mPFC neurons were strongly modulated during behaviour in a way that seemed to specifically reflect the decision to act or refrain from action during the FST. An example neuron is shown (Fig. 2c, d). This neuron was highly active during the mostly immobile pre- and post-FST epochs (98% and 94% immobile, respectively), but during the FST it stayed active during mobile states and was inhibited during immobile states. This neuron did not simply encode locomotor activity but was instead specifically inhibited during FST immobility corresponding to traditionally defined states of behavioural despair[18].

Many neurons in the recorded population (23 out of 160, 14%; see Supplementary Methods) exhibited this surprising profile of activity. All rats exhibited minimal motor activity during the pre-FST epoch (greater than 88% immobility for all rats, average 97% immobility) and a moderate to high level of motor activity during the FST epoch (less than 79% immobility for all rats, average 39% immobility, Fig. 2e). Most recorded neurons (129 out of 160, 81%) showed a significant change in firing rate between pre-FST and FST epochs (Fig. 2f, top; statistics described in Fig. 2c and Methods). On average, this population of neurons was inhibited during the FST epoch (80 out of 129, 62%). Many neurons (70 out of 160, 44%) also showed a difference in firing rate between mobile and immobile states within the FST epoch (Fig. 2f, bottom). Most of these neurons were activated during mobile states and inhibited during immobile states (51 out of 70, 73%).
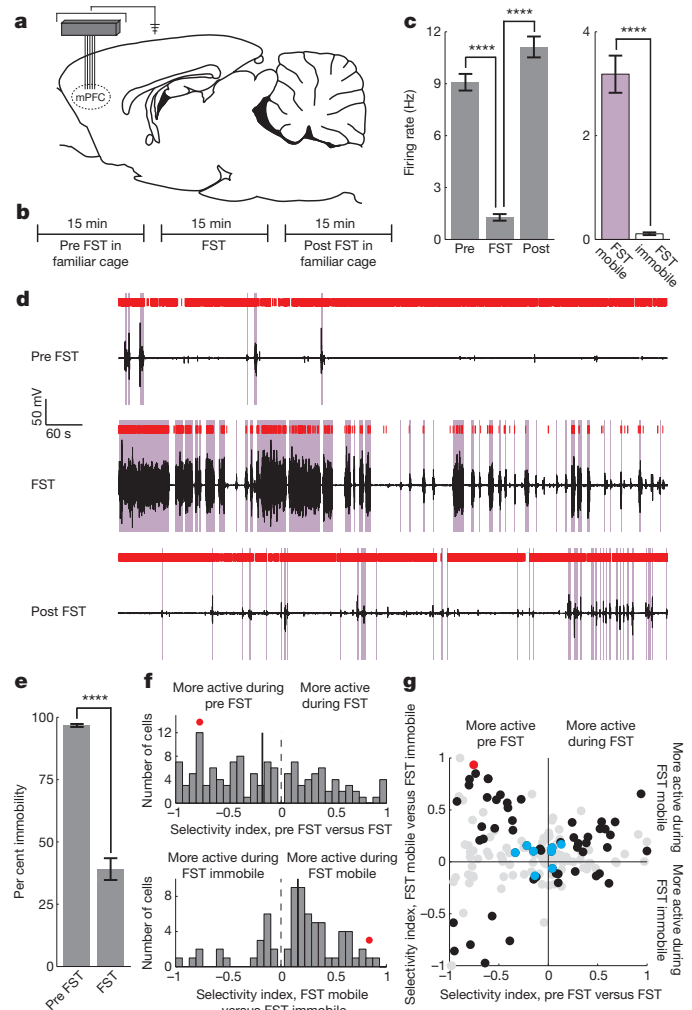

Figure 2 | Prefrontal neuronal activity encodes FST behavioural state. a, A tetrode microdrive or fixed wire array was implanted over the mPFC. **b**, Data were recorded pre FST, during the FST and post FST (for 15 min each). **c**, Bar plot of an example neuron that is inhibited during immobile states in the FST (Mann–Whitney U-test, $*P < 0.05$; $**P < 0.01$; $***P < 0.001$; $****P < 0.0001$). **d**, Raster plot of the same neuron as in **c**. Coil voltage in black, mobile states in purple, spikes in red. Top, pre-FST activity; middle, activity during the FST; bottom, post-FST activity. **e**, Immobility during the pre-FST and FST test epochs (11 rats). **f**, Distribution of population selectivity indices (Supplementary Methods). Top, pre FST versus FST epochs. All neurons significantly selective for pre FST versus FST (as in panel **c**) are shown. Bottom, mobile versus immobile FST states. All neurons significantly selective for mobile versus immobile FST state are shown. **g**, Joint distribution of selectivity indices. Black circles, neurons selective for both task epoch and mobility; red circle, example neuron; blue circles, putative inhibitory fast-spiking neurons; grey circles, non-significantly selective neurons. All recorded neurons are shown. Error bars indicate s.e.m.

We then examined the joint distribution of epoch- and mobility-dependent neural selectivity among four quadrants (Fig. 2g), and found it to be highly asymmetric. The upper right and lower left quadrants exhibited a straightforward correspondence between motor activity and neural activity; for example, neurons in the upper right quadrant were more active during the largely mobile FST epoch than during the immobile pre-FST epoch, and, within the FST epoch, were more active during mobile states. The other two quadrants (the upper left and lower right quadrants) showed an inverted correspondence. In the upper left quadrant, neurons that were quieted during the more-active FST epoch were actually activated during escape behaviours within FST, but the opposite was true for neurons in the lower right quadrant. The profile of activity found within these groups was therefore not simply dependent on motor activity. We noted that putative

fast-spiking interneurons (Supplementary Methods) exhibited a reduced degree of modulation along both selectivity dimensions. Finally, we found that when mPFC neural activity was aligned to the onset of mobility epochs, firing on average preceded the onset of mobility (Supplementary Fig. 3).

The mPFC neurons that we recorded exhibited a range of selectivity profiles; therefore, it was not obvious that optogenetically activating local neurons in the mPFC would have a net effect on behaviour during the FST. To test this, we restricted opsin expression to Ca^{2+}/calmodulin-dependent protein kinase-α (CaMKIIα)-expressing (chiefly excitatory) neurons within the mPFC using an adeno-associated viral vector (AAV5) expressing channelrhodopsin-2 fused to enhanced yellow fluorescent protein (ChR2–eYFP) under the control of the CaMKIIα promoter. Virus was infused into the mPFC and fibre optics were implanted over the mPFC (Fig. 3a, b). We confirmed functional targeting of these neurons with optrode recordings in the mPFC under anaesthetic (Supplementary Fig. 4a), but surprisingly, when these neurons were illuminated in 2-min epochs during the FST (Supplementary Methods), we found that stimulation was not sufficient to cause even a slight reduction in FST immobility (Fig. 3c, Wilcoxon signed-rank test, $P = 0.23$) or a change in a control open-field-test (OFT) behaviour (Supplementary Fig. 4b). One interpretation of these results is that local mPFC neurons may correlate with, but are not causally involved in, the behavioural state

changes associated with effort-related mobility and immobility; alternatively, it could be that some local mPFC neurons are involved in this way, but others are not or are opposed in causal function, and when driven together no net effect on behaviour is seen. We therefore next considered that it could be possible to induce a change in this motivated behavioural state by restricting optogenetic stimulation to a reduced population of mPFC neurons.

The mPFC is known to project to several downstream brain regions that have been implicated in motivated behaviour and depression[21]; among these is the dorsal raphe nucleus (DRN)[22], a serotonergic nucleus implicated in major depressive disorder[4]. The mPFC exerts control over both neural activity in the DRN and extracellular 5-hydroxytryptamine (5-HT; serotonin) levels[15,23], and antidepressant-like effects of mPFC electrical stimulation seem to depend on an intact 5-HT system[13], but the projection from the mPFC to the DRN has not been directly shown to have an effect on behaviour. To specifically activate the mPFC–DRN projection, we first transduced excitatory neurons in the mPFC with AAV5 CaMKIIα::ChR2–eYFP (Fig. 3d), which led to robust ChR2–eYFP expression in mPFC axons in the DRN (Fig. 3e and Supplementary Fig. 5a). We restricted activation to the subpopulation of excitatory neurons in the mPFC that project to the DRN by implanting a fibre optic over the DRN and selectively illuminating this region (Fig. 3d). We confirmed functional
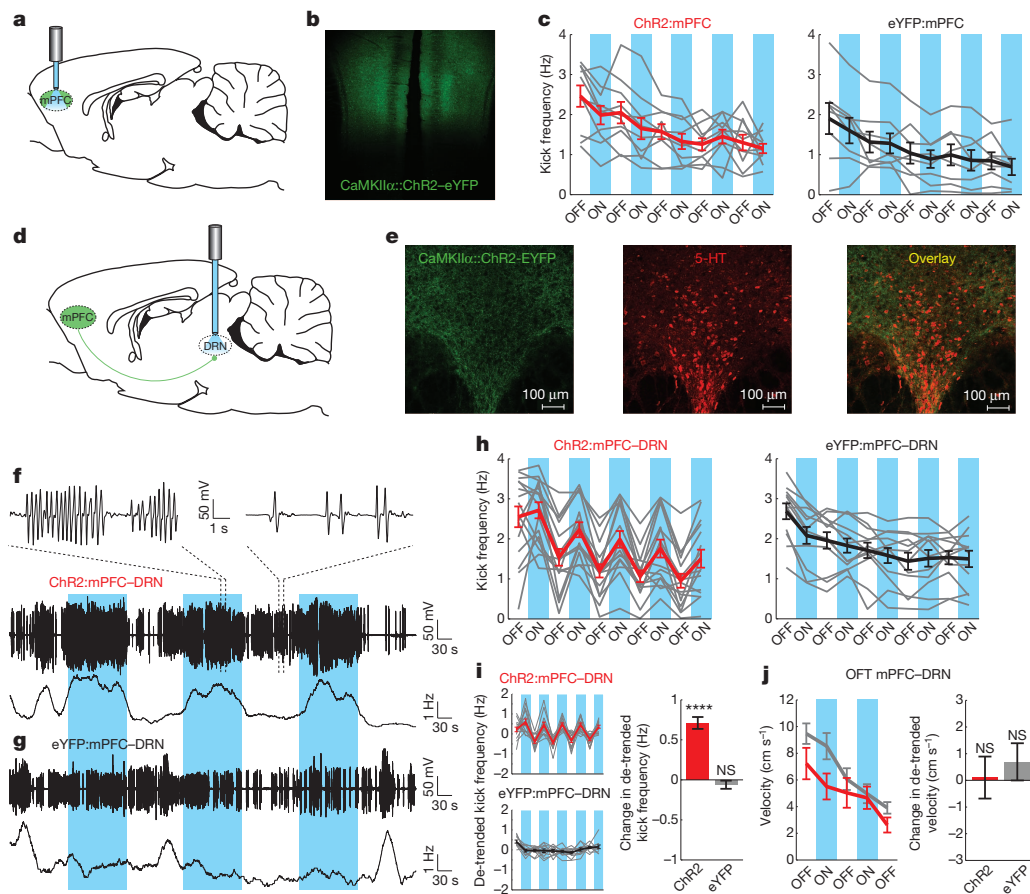

Figure 3 | Optogenetic stimulation of mPFC axons in the DRN, but not excitatory mPFC cell bodies, induces behavioural activation. a, ChR2–eYFP or eYFP-expressing mPFC principal neurons were illuminated directly. **b**, ChR2–eYFP fluorescence in the mPFC. **c**, FST kick frequency for the ChR2 in mPFC condition (ChR2:mPFC) (left, $n = 10$) and the eYFP in mPFC condition (eYFP:mPFC) (right, $n = 8$) rats. Grey lines, individual rats; thick lines, average for ChR2:mPFC (red) or EYFP:mPFC (black) rats; blue bars, light on. **d**, A fibre optic was implanted over the DRN after mPFC injection. **e**, ChR2–eYFP fluorescence in mPFC axons in the DRN (immunostained for 5-HT). **f**, FST behavioural data from one ChR2:mPFC–DRN rat. Top and middle, coil

voltage; bottom, kick frequency. **g**, FST data from one eYFP:mPFC–DRN rat. **h**, FST kick frequency for all rats. Left, ChR2:mPFC–DRN rats ($n = 16$); right, eYFP:mPFC–DRN rats ($n = 12$). **i**, Left, exponentially de-trended data from **h**; right, change in de-trended kick frequency from light-off to light-on epochs, ChR2:mPFC–DRN (red) and eYFP:mPFC–DRN (grey) rats. **j**, Left, velocity during stimulation in the open field test; right, change in de-trended velocity from light-off to light-on epochs. Red, ChR2:mPFC–DRN rats ($n = 12$); grey, eYFP:mPFC–DRN rats ($n = 12$). NS, not significant. Error bars indicate s.e.m.

targeting with optrode recordings under anaesthetic (Supplementary Fig. 5b).

When the axons of ChR2–eYFP-expressing mPFC neurons in the DRN were stimulated during the FST, a profound change in effortful behaviour resulted. Example induction-coil behavioural traces from two rats are shown (one ChR2–eYFP and one eYFP rat, Fig. 3f, g), demonstrating a robust increase in kick frequency during each light epoch in the ChR2–eYFP case. This behavioural effect was present in most ChR2–eYFP rats (Wilcoxon signed-rank test, $P = 1.04 \times 10^{-11}$) but not eYFP rats (Wilcoxon signed-rank test, $P = 0.39$), and was rapid, reversible and repeatable (Fig. 3h, i). Importantly, stimulation of this projection did not affect non-specific locomotor activity in the open field in either ChR2–eYFP rats (Wilcoxon signed-rank test, $P = 0.59$) or EYFP rats (Wilcoxon signed-rank test, $P = 0.71$, Fig. 3j). This result shows the importance of resolving neural subpopulations *in vivo* defined by anatomical presence of axonal projection target region, and illustrates a causal role of a specific mPFC-to-brainstem neural pathway in driving this motivated behavioural response to a challenging environment. Additional experiments addressing the effect of mPFC–DRN stimulation on mPFC neural activity are described in Supplementary Figs 6–9.

The mPFC projection to the DRN sends sparse collaterals to other brain regions[24]; accordingly, we next blocked incoming glutamatergic synaptic activity in the DRN during stimulation of DRN-projecting mPFC axons (Supplementary Fig. 10). Glutamate receptor antagonists blocked stimulation-driven behavioural activation, consistent with the idea that activation of the mPFC–DRN synapse itself is necessary for the stimulation-induced increase in mobility. Additionally, inhibition of mPFC axons in the DRN led to a lasting decrease in steady-state mobility in the FST (Supplementary Fig. 11), pointing to the necessity of this pathway in normal behaviour.

We considered the possibility that specificity of the effect of mPFC on DRN would not be fully captured by general activation of the downstream region; we tested this question directly by transducing neurons in the DRN with ChR2–eYFP under the control of the human synapsin 1 promoter (AAV5 human synapsin promoter fragment (hSyn)::ChR2–eYFP), which transduced both 5-HT and GABA (γ-aminobutyric acid) neurons in the DRN (Supplementary Fig. 12), and implanted a fibre optic directly above the DRN (Fig. 4a–c). When ChR2–eYFP-expressing DRN cell bodies were illuminated directly, rats exhibited behavioural activation during the FST (Wilcoxon signed-rank test, $P = 5.63 \times 10^{-8}$), whereas eYFP-expressing rats did not (Wilcoxon signed-rank test, $P = 0.84$, Fig. 4d, e). However, direct activation of the DRN, unlike stimulation of the mPFC–DRN projection, led to a general increase in locomotor activity in the OFT in ChR2–eYFP rats (Wilcoxon signed-rank test, $P = 0.02$) but not eYFP rats (Wilcoxon signed-rank test, $P = 0.31$, Fig. 4f). It is likely that mPFC–DRN stimulation and direct DRN-cell-body stimulation activate different sub-networks within the DRN, which may explain these dissimilar behavioural results.

Finally, we targeted the projection from the mPFC to the lateral habenula[25], a region known to have an important role in motivated behaviour and depression[26,27], and found that activation of this specific projection had the opposite effect on escape-related behaviour in the FST. As above, we infused AAV5 CaMKIIα::ChR2–eYFP into the mPFC and implanted bilateral fibre optics over the lateral habenula (Fig. 4g–i). When ChR2–eYFP-expressing lateral-habenula-projecting mPFC axons were illuminated during the FST, rats showed a rapid and reversible decrease in mobility (Wilcoxon signed-rank test, $P = 3.63 \times 10^{-4}$), whereas control eYFP-expressing rats did not (Wilcoxon signed-rank test, $P = 0.29$, Fig. 4j–l, Supplementary Fig. 13).

Here, we have probed both neural correlates and causal neural pathways involved in the selection of an effortful motivated behavioural pattern during challenging circumstances, using novel technology that permits electrical recordings and optogenetic control in the FST in combination with high-speed reporting of behavioural state. We
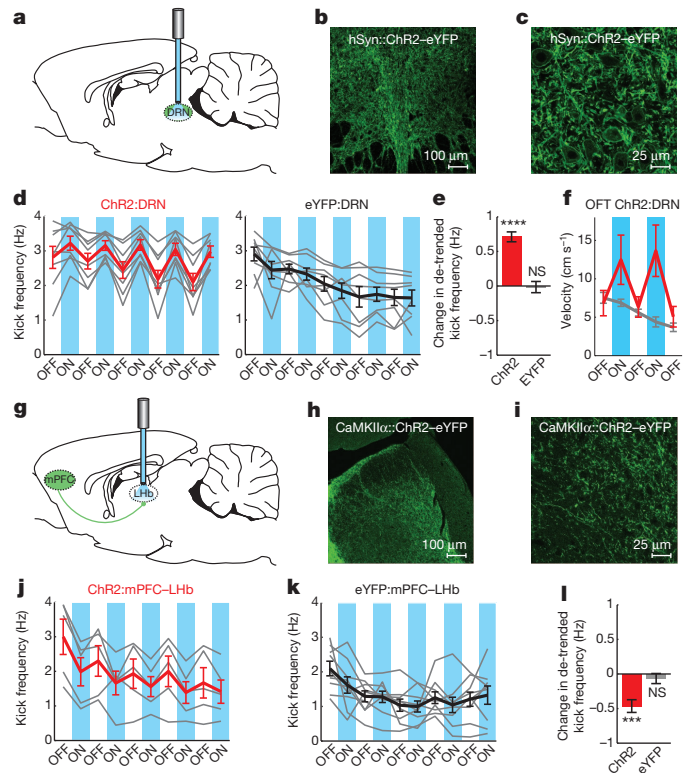

Figure 4 | Behavioural activation resulting from stimulation of DRN-projecting mPFC axons is specific to the mPFC–DRN synapse. a, A fibre optic was implanted over ChR2- or eYFP-expressing neurons in the DRN. **b,** Image (×20) of ChR2–eYFP-expressing DRN neuronal cell bodies. **c,** DRN image. **d,** FST kick frequency for all rats. Left, ChR2:DRN rats ($n = 8$); right, eYFP:DRN rats ($n = 8$); grey lines, individual rats; thick lines, average for ChR2:DRN (red) or eYFP:DRN (black) rats; blue bars, light on. **e,** De-trended change in kick frequency from light-off to light-on epochs, ChR2:DRN (red) and eYFP:DRN (grey) rats. **f,** Velocity during stimulation in the open field test. Red, ChR2:DRN ($n = 12$); grey, eYFP:DRN ($n = 12$) rats. **g,** Fibre optics were implanted bilaterally over the lateral habenula (LHb) to activate ChR2-expressing LHb-projecting mPFC axons. **h,** ChR2–eYFP-expressing mPFC axons in the LHb. **i,** LHb image. **j,** FST kick frequency for all rats. Left, ChR2:mPFC–LHb rats ($n = 5$); right, eYFP:mPFC–LHb rats ($n = 9$). **k,** De-trended change in kick frequency from light-off to light-on epochs in the FST. Error bars indicate s.e.m.

have shown the existence of different physiologically defined mPFC neural populations—one selectively inhibited during passive coping/behavioural despair-like states, and the other selectively activated during these states. We have also shown that, although general activation of CaMKIIα-expressing neurons in the mPFC does not have a net effect on this behaviour in rats, selective activation in DRN or lateral habenula of projecting mPFC neurons elicits distinct, rapid and reversible effects on selection of the active behavioural state. These results describe the neural dynamics associated with the behavioural response to challenge and demonstrate the causal importance of mPFC control of downstream targets in implementing this response, with implications for understanding both normal and pathological states of decision pathway refinement, likely-outcome assessment, and behavioural pattern selection.

METHODS SUMMARY

Male Long-Evans rats were implanted with either a 4-tetrode microdrive or a 24-electrode fixed wire array targeted to the mPFC. Tetrodes were adjusted daily. Prior to the start of recordings rats were anaesthetized for 10 min to facilitate waterproofing of the headstage and electrodes, and were subsequently allowed to recover for at least 1 h. Data were analysed in Matlab and Neuroexplorer with custom-written software.

The pAAV–CaMKIIα::hChR2(H134R)–eYFP, pAAV–CaMKIIα::eYFP, pAAV–CaMKIIα::eNpHR3.0–eYFP and pAAV–hSyn::hChR2(H134R)–eYFP plasmids were designed and constructed by standard methods and packaged as AAV5. Virus was injected into the mPFC or the DRN. Maps and clones are available at http://www.stanford.edu/group/dlab/optogenetics.

The mPFC was virally transduced and an optical fibre was surgically implanted in separate surgeries over the DRN or the lateral habenula to allow for selective illumination of mPFC axons. Cannulae were used instead for pharmacology experiments. Virus was allowed to express for a minimum of 4 months after injection for projection-targeting experiments. Behavioural data were collected 7–10 days after fibre implantation.

To confirm opsin expression, coronal brain slices were prepared for immunohistochemistry and optical microscopy. Brain sections were stained for 4′,6-diamidino-2-phenylindole (DAPI) and either rabbit anti-5-HT or rabbit anti-GABA. Sections were imaged with a confocal microscope.

1. McGuire, J. T. & Botvinick, M. M. Prefrontal cortex, cognitive control, and the registration of decision costs. *Proc. Natl Acad. Sci. USA* **107,** 7922–7926 (2010).
2. Ridderinkhof, K. R., van den Wildenberg, W. P. M., Segalowitz, S. J. & Carter, C. S. Neurocognitive mechanisms of cognitive control: the role of prefrontal cortex in action selection, response inhibition, performance monitoring, and reward-based learning. *Brain Cogn.* **56,** 129–140 (2004).
3. Mayberg, H. S. *et al.* Reciprocal limbic-cortical function and negative mood: converging PET findings in depression and normal sadness. *Am. J. Psychiatry* **156,** 675–682 (1999).
4. Maes, M. & Meltzer, H. In *Psychopharmacology: the Fourth Generation of Progress* (eds Bloom, F. E. & Kupfer, D. J.) 933–944 (Raven Press, 1995).
5. Kessler, R. C. *et al.* Lifetime prevalence and age-of-onset distributions of mental disorders in the World Health Organization's World Mental Health Survey Initiative. *World Psychiatry* **6,** 168–176 (2007).
6. Miller, E. K. & Cohen, J. D. An integrative theory of prefrontal cortex function. *Annu. Rev. Neurosci.* **24,** 167–202 (2001).
7. Fuster, J. M. *The Prefrontal Cortex, Fourth Edition* (Academic Press, 2008).
8. Elliott, R. *et al.* Prefrontal dysfunction in depressed patients performing a complex planning task: a study using positron emission tomography. *Psychol. Med.* **27,** 931–942 (1997).
9. Austin, M.-P. Cognitive deficits in depression: possible implications for functional neuropathology. *Br. J. Psychiatry* **178,** 200–206 (2001).
10. Ingram, R. E., Bernet, C. Z. & McLaughlin, S. C. Attentional allocation processes in individuals at risk for depression. *Cognit. Ther. Res.* **18,** 317–332 (1994).
11. Dalgleish, T. & Watts, F. N. Biases of attention and memory in disorders of anxiety and depression. *Clin. Psychol. Rev.* **10,** 589–604 (1990).
12. Mayberg, H. S. *et al.* Deep brain stimulation for treatment-resistant depression. *Neuron* **45,** 651–660 (2005).
13. Hamani, C. *et al.* Antidepressant-like effects of medial prefrontal cortex deep brain stimulation in rats. *Biol. Psychiatry* **67,** 117–124 (2010).
14. Covington, H. E. *et al.* Antidepressant effect of optogenetic stimulation of the medial prefrontal cortex. *J. Neurosci.* **30,** 16082–16090 (2010).
15. Amat, J. *et al.* Medial prefrontal cortex determines how stressor controllability affects behavior and dorsal raphe nucleus. *Nature Neurosci.* **8,** 365–371 (2005).
16. Drevets, W. C. Neuroimaging and neuropathological studies of depression: implications for the cognitive-emotional features of mood disorders. *Curr. Opin. Neurobiol.* **11,** 240–249 (2001).
17. Baxter, L. R. *et al.* Reduction of prefrontal cortex glucose metabolism common to three types of depression. *Arch. Gen. Psychiatry* **46,** 243–250 (1989).
18. Porsolt, R. D., Le Pichon, M. & Jalfre, M. Depression: a new animal model sensitive to antidepressant treatments. *Nature* **266,** 730–732 (1977).
19. Cryan, J. F., Valentino, R. J. & Lucki, I. Assessing substrates underlying the behavioral effects of antidepressants using the modified rat forced swimming test. *Neurosci. Biobehav. Rev.* **29,** 547–569 (2005).
20. Willner, P. Chronic mild stress (CMS) revisited: consistency and behavioural-neurobiological concordance in the effects of CMS. *Neuropsychobiology* **52,** 90–110 (2005).
21. Vertes, R. P. Differential projections of the infralimbic and prelimbic cortex in the rat. *Synapse* **51,** 32–58 (2004).
22. Gonçalves, L., Nogueira, M. I., Shammah-Lagnado, S. J. & Metzger, M. Prefrontal afferents to the dorsal raphe nucleus in the rat. *Brain Res. Bull.* **78,** 240–247 (2009).
23. Celada, P., Puig, M. V., Casanovas, J. M., Guillazo, G. & Artigas, F. Control of dorsal raphe serotonergic neurons by the medial prefrontal cortex: involvement of serotonin-1A, GABA(A), and glutamate receptors. *J. Neurosci.* **21,** 9917–9929 (2001).
24. Gabbott, P. L. A., Warner, T. A., Jays, P. R. L., Salway, P. & Busby, S. J. Prefrontal cortex in the rat: projections to subcortical autonomic, motor, and limbic centers. *J. Comp. Neurol.* **492,** 145–177 (2005).
25. Kim, U. & Lee, T. Topography of descending projections from anterior insular and medial prefrontal regions to the lateral habenula of the epithalamus in the rat. *Eur. J. Neurosci.* **35,** 1253–1269 (2012).
26. Matsumoto, M. & Hikosaka, O. Representation of negative motivational value in the primate lateral habenula. *Nature Neurosci.* **12,** 77–84 (2009).
27. Sartorius, A. *et al.* Remission of major depression under deep brain stimulation of the lateral habenula in a therapy-refractory patient. *Biol. Psychiatry* **67,** e9–e11 (2010).